Data-based hydrodynamic coefficients interpolation for control co-design of wave energy converters

Demián García-Violini, Yerai Peña-Sanchez, Ander Zarketa, & Markel Penalba

Abstract—**A control co-design (CCD) scheme is an approach that involves integrating control strategies into the overall design process, particularly considered in wave energy systems. When considering geometrical optimisation in CCD schemes, one of the challenges is the computational demand associated with recomputing hydrodynamic coefficients for each design iteration. To overcome this challenge, an efficient solution based on an advanced data-based interpolation model is presented in this study. The interpolation model utilises an extended base case dataset, including hydrodynamic coefficients for a range of expected variations. By leveraging this dataset, accurate information on hydrodynamic variations beyond the base case can be obtained, significantly reducing the computational cost of a CCD structure. Thus, a CCD scheme, which integrates a spectral-based energy-maximising control strategy with an interpolation-based geometric optimisation routine, is presented in this study. Overall, this paper contributes to the advancement of CCD strategies in the development of economically viable wave energy conversion systems.**

Index Terms—**Wave Energy, Control co-design, Hydrodynamic coefficients, Interpolation, Extrapolation**

I. Introduction

Ocean waves store an enormous amount of untapped energy. Various developers, members of the R&D community, have suggested diverse prototypes of wave energy converters (WECs) based on different energy absorption principles. Some of these WECs have demonstrated their technical viability through the testing of reduced-scale prototypes in wave tanks and the deployment of near-full-scale prototypes in the open ocean (see, for example, the M4 device [1]), showcasing their energy-absorbing capabilities. Additionally, a few prototypes have proven the reliability of their concepts by successfully enduring extreme events during open ocean testing. However, despite these achievements, none of these prototypes has demonstrated economic viability, indicating their lack of readiness to compete against other energy sources in the market.

In order to improve the economic viability of these devices, two main actions have been identified. On the one hand, the energy absorption capability of the devices must be enhanced, for which the design of advanced energy-maximising control strategies is crucial. On the other hand, cost reduction, both capital and operational expenditures, i.e. CapEx and OpEx, respectively, is a key action, meaning that more reliable prototypes must be designed from an economic perspective. In the traditional design process, the most critical aspects of WECs, *i.e.* the absorbing mechanism (floater), the power take-off (PTO) system, and mooring lines, are optimised based on the energy absorption capabilities and the loading on critical elements, generally driven by a simplified control strategy, most commonly based on an unconstrained passive resistive control represented by a 'damping'. As a common and well-established practice in the R & D community, once the WEC design is determined, an advanced control strategy is developed to maximise energy absorption and generation capabilities [2], while the physical integrity of the system is preserved, through active constraint handling mechanisms.

However, by implementing more sophisticated and aggressive control actions, the behaviour of the WEC is significantly altered, resulting in a substantial enhancement of its motion. Consequently, the originally designed dimensions of the absorber, power take-off (PTO) system, and mooring lines may not be suitable for the behaviour exhibited under a more sophisticated control strategy. To address this mismatch between the original WEC design and the observed behaviour resulting from the advanced control solution, the control strategy is adapted to maximise the energy extraction within the constraints of the design, although it may not be optimal [3]. Furthermore, it is possible that the design characteristics include unnecessary design redundancies and over-dimensioning, which can have a negative impact on the final CapEx and OpEx of the

Demián García-Violini is supported by the Agencia I+D+i from the Government of Argentina under grant PICT-2021-I-INVI-00190.

Markel Penalba and Ander Zarketa-Astigarraga are funded by *MCIN/AEI/10.13039/501100011033 ERDF A way of making Europe* under the Grant PID2021-124245OA-I00 and by the Basque Government's ELKARTEK 2022 program under Grant KK-2022/00090.

Yerai Peña-Sanchez is funded by the European Union's Horizon 2020 research and innovation programme under the Marie Sklodowska-Curie grant agreements N°101034297.

Demián García-Violini is with Departamento de Ciencia y Tecnología, Universidad Nacional de Quilmes, Roque Saenz Peña 352, Bernal B1876, Argentina, Consejo Nacional de Investigaciones Científicas y Técnicas (CONICET), Argentina, and Center for Ocean Energy Research, Maynooth University, Maynooth W23 F2H6, Ireland, (e-mail: ddgv83@gmail.com).

Yerai Peña-Sanchez is with Euskal Herriko Unibertsitatea (EHU/UPV), Bizcaia, Spain (e-mail: yerai.pena@ehu.eus, corresponding author).

Ander Zarketa is with Fluid Mechanics, Mondragon University, Loramendi 4, 20500 Arrasate, Spain. (e-mail: azarketa@mondragon.edu).

Markel Penalba is with Fluid Mechanics, Mondragon University, Loramendi 4, 20500 Arrasate, Spain, and Ikerbasque, Basque Foundation for Science, Euskadi Plaza 5, Bilbao, Spain. (e-mail: mpenalba@mondragon.edu).

Digital Object Identifier: https://doi.org/10.36688/ewtec-2023-534

WEC system.

To mitigate such problems, an alternative design approach has been introduced in the literature, which involves incorporating a general control methodology into the overall design of the WEC, from an early stage. This approach, commonly referred to in the literature as control co-design (CCD) [4], aims to address the integration of control strategies during the design process. Consequently, considering a CCD paradigm, the design of the absorber dimensions and shape [4], as well as the PTO constraints [5], among other aspects, can be determined by taking into account the behaviour of the device under the action of a general control strategy. To summarise, this design paradigm describes an approach where optimisation is carried out in a *control-aware* manner. By way of example, in [6] and [7] the interaction between optimal array layout and control is demonstrated, while the study in [8] discusses the interaction between control and optimal WEC geometry. In particular, as discussed in [4], CCD strategies can play a significant contribution in achieving an optimal structural design for the absorber geometry, aligning it with the energy-maximising control scheme. However, analysing and redesigning geometry variations within a CCD loop requires a recomputation of hydrodynamic coefficients, to update the WEC geometry, which implies running a boundary element method (BEM) software at each iteration. Thus, even for WECs with relatively simple geometrical complexity, the computational demand of the CCD optimisation loop can become prohibitive. In such cases, the only viable solution may involve reducing the resolution of the BEM simulation, specifically, through a reduction in geometry discretisation or the number of frequencies. This adjustment aims to make the CCD optimisation numerically feasible. Another potential solution is to compute an extensive pre-defined database of hydrodynamic coefficients that covers all potential geometry variations in advance. Alternatively, a reduced database combined with an interpolator can be utilised to address the issue. This approach has been suggested in the literature [9], [10], although its application within a CCD approach has not been explored. It is important to note that the computation of hydrodynamic coefficients represents a significant barrier to the implementation of general CCD schemes in the development of WEC technologies.

Within this context, the present paper suggests an alternative efficient solution for the computation of hydrodynamic coefficient in CCD loops, which avoids the need for using BEM methods in CCD schemes. Based on an advanced data-based interpolation model for identifying the hydrodynamic coefficients for any variation of a base case geometry. To that end, the interpolation model is provided with hydrodynamic data for an extended base case, including the coefficients for the base case geometry and a limited range of expected variations. Based on this extended space, the data-based interpolator provides accurate information on any variations beyond the original base case, significantly reducing the computational cost of the CCD approach. Furthermore, this study explores alternative methodologies to tackle CCD problems, with a particular focus on employing a binary search approach to solve the considered CCD problem. Thus, the binary approach considered leverages the utilisation of precomputed interpolating (or alternatively fitting functions) obtained from a database. Additionally, a case study is presented, showcasing the practical application of the methodology across the entire problem domain.

The remainder of this paper is organised as follows. The basics of WEC modelling are recalled in Section II. The spectral control approach considered in the CCD scheme, to maximise energy absorption while preserving a set of physical constraints, is presented in Section III. The considered interpolation-based order reduction technique for computing hydrodynamic coefficients, to reduce the computational complexity while accurately capturing the system dynamics, is introduced in Section IV. In Section V, the reduced-order structural optimisation CCD approach is presented, highlighting the considerations for achieving an optimal absorber geometry aligned with the energy-maximising control scheme. A case study is presented in Section VI, where the proposed approach is applied to a generic, full-scale, realistic WEC system. Finally, Section VII concludes the paper, summarising the key findings, and discussing the implications of the presented approach.

II. WECs: Modelling framework

The dynamic model of a WEC system, which captures the interaction between acting hydrodynamic forces and motion of a floating body, is described by the well-established Cummins' equation, a widely adopted theoretical framework [11]. By applying this formulation, which is essentially based on Newton's second law, the dynamic behaviour of a general WEC system can be characterised. In this study, a single degree-of-freedom (DoF) WEC is considered, without loss of generality. The model of a WEC can be defined as follows:

$$(M + A_\infty)\,\ddot{x}(t) = f_{ex}(t) - f_{\mathrm{r}}(t) - f_{\mathrm{h}}(t) - f_{\mathrm{u}}(t). \quad (1)$$

In Eq. (1), M denotes the mass of the body, while x, $\dot{x}$ (v), and $\ddot{x}$ (a) represent the position, velocity, and acceleration of the WEC device, respectively. The radiation force, denoted as $f_{\mathrm{r}}(t)$, is given by the convolution integral $k_{\mathrm{r}}(t) * v(t)$, where $k_{\mathrm{r}}(t)$ represents the impulse response of the radiation force. The restoring force, caused by buoyancy, is expressed as $f_{\mathrm{h}}(t) = s_{\mathrm{h}} x(t)$, where s_{h} represents the hydrostatic stiffness. The control force, generated by the action of a power take-off (PTO) system, is denoted as $f_{\mathrm{u}}(t)$, while $f_{ex}(t)$ corresponds to the excitation force. In Eq. (1), A_∞ refers to the added mass at infinite frequency, defined as $A_\infty = \lim_{\omega\to+\infty} A_{\mathrm{r}}(\omega)$, where $A_{\mathrm{r}}(\omega)$ and $B_{\mathrm{r}}(\omega)$ represent the radiation added-mass and damping, respectively. Both $A_r(\omega)$ and $B_r(\omega)$, in the spectral domain,

are determined using Ogilvie's relations [12], given by:

$$\begin{aligned} A_{\mathrm{r}}(\omega) &= A_\infty - \tfrac{1}{\omega}\int_0^{+\infty} k_{\mathrm{r}}(t)\sin(\omega t)dt, \\ B_{\mathrm{r}}(\omega) &= \int_0^{+\infty} k_{\mathrm{r}}(t)\cos(\omega t)dt. \end{aligned} \tag{2}$$

Using Eq. (2), the radiation convolution kernel can be described as follows:

$$H_{\mathrm{r}}(\omega) = B_{\mathrm{r}}(\omega) + \jmath\omega\left[A_{\mathrm{r}}(\omega) - A_\infty\right], \tag{3}$$

where $k_{\mathrm{r}}(t)$ and $H_{\mathrm{r}}(\omega)$ are a Fourier transform pair. Using Eq.(3), Eq.(1) can be expressed in the frequency domain, considering a force-to-velocity description [13], as:

$$V(\omega) = \frac{1}{Z_i(\omega)}\left[F_{ex}(\omega) - F_u(\omega)\right], \tag{4}$$

with

$$Z_i(\omega) = B_{\mathrm{r}}(\omega) + \jmath\omega\left(M + A_{\mathrm{r}}(\omega) - \frac{s_{\mathrm{h}}}{\omega^2}\right), \tag{5}$$

the mechanical impedance of the system.

Thus, using Eq. (5), the standard force-to-velocity, which represents a key driver for control design purposes, can be represented in terms of a transfer function [14], given by:

$$G(\omega) = \frac{\jmath\omega}{(\jmath\omega)^2(M + A_\infty) + (\jmath\omega)H_{\mathrm{r}}(\omega) + s_{\mathrm{h}}} = \frac{1}{Z_i(\omega)}. \tag{6}$$

In particular, in Eq. (6), $H_{\mathrm{r}}(\omega)$ is typically computed using boundary-element methods such as NEMOH [15]. Additionally, for general purposes, such as control, an LTI-based approximating representation $\hat{H}_{\mathrm{r}}(s) \approx H_{\mathrm{r}}(\omega)$ for $s = \jmath\omega$, where $\hat{H}_{\mathrm{r}}(s)$ is a stable linear time-invariant (LTI) system, is generally considered in the literature [14], which can be obtained using advanced system identification software, such as FOAMM [16].

Finally, under the wave excitation force $f_{\mathrm{ex}}(t)$ is modelled in the spectral domain, simultaneously with the procedure performed for, for example, $A_{\mathrm{r}}(\omega)$ and $B_{\mathrm{r}}(\omega)$, using BEM-based tools. Thus, a mapping from the wave-heigh elevation, $\eta(t)$, to the excitation force, $f_{\mathrm{ex}}(t)$, is defined as $\mathcal{H}_{\mathrm{ex}}(\omega)$.

III. Spectral Control Approach

As mentioned in the introduction, Section I, a CCD scheme, for geometrical structure design aligned, from an optimal perspective, with a specific control strategy, is presented in this study [17]. To this aim, this section outlines the foundations of spectral-based control strategies. From a general perspective, spectral controllers are optimisation-based control schemes, which compute an optimal control input by solving an optimisation problem and can, therefore, deal with physical constraints obtaining (theoretically) optimal solutions [18]. Thus, a spectral-based controller can ensure optimal power capture, while, at the same time, the performance of the controller under realistic motion and PTO force ranges, i.e. position and control force constraints, is studied. To this aim, in Sections III-A and III-B the general control objective in WECs and the foundations of spectral controllers are recalled, respectively.

A. Control Objective

The control objective in a general WEC control problem is to maximise the total absorbed energy. For a WEC system, which is subject to an external excitation force $f_{ex}(t)$ and is controlled via the PTO force $f_{\mathrm{u}}(t)$, the total absorbed energy, over the interval $[0\ T]$, is computed as:

$$E = -\int_0^T P(t)dt = -\int_0^T v^\intercal(t) f_{\mathrm{u}}(t)dt, \tag{7}$$

where $P(t)$ is the instantaneous power, and $f_{\mathrm{u}}(t)$ and $v(t)$ are the control force and device velocity, respectively, both introduced in Eq (1). Thus, the general control problem is defined as,

$$\begin{aligned} \max_{f_{\mathrm{u}}(t)} \quad & -\int_0^T v(t)^\intercal f_{\mathrm{u}}(t)dt \\ \text{subject to} \quad & \begin{cases} \dot{\mathrm{x}} = \mathcal{F}(\mathrm{x}, f_{\mathrm{u}}, f_{\mathrm{ex}}) \\ v = \mathcal{G}(\mathrm{x}) \\ \mathcal{C} \end{cases} \end{aligned} \tag{8}$$

where $\mathcal{F}(x, f_{\mathrm{u}}, f_{\mathrm{ex}})$ denotes the state-space representation of the system in Eq. (1), $\mathcal{G}(\mathrm{x})$ the output mapping $\mathrm{x} \mapsto v$, and $\mathcal{C}$ a general set of constraints (such as displacement constraints $x_{min} \leq x(t) \leq x_{max}$, or PTO force constraints $f_{min} \leq f_{\mathrm{u}}(t) \leq f_{max}$, etc.), specifically defined for each WEC control problem.

B. (Pseudo-)spectral Approximation

In this study, a control methodology based on (pseudo-)spectral techniques is considered for the control problem described in Eq. (8). To be precise, (pseudo)-spectral control refers to a control approach that utilises (pseudo)-spectral methods for control systems analysis and design [17]. (Pseudo)-spectral methods are numerical techniques that involve the approximation of functions using a set of specific basis functions, such as Fourier, Legendre or Chebyshev polynomials. Specifically, in the context of control, (pseudo)-spectral control aims to represent the dynamics of a system using these basis functions and leverage their properties for control design. Considering (pseudo)-spectral methods, the representation of system dynamics with high accuracy can be achieved, enabling precise analysis and design of control strategies. In particular, (pseudo)-spectral control has been widely applied to WEC systems as in, for example, [17] or [19]. With the aim of applying (pseudo)-spectral control in the presented study, the optimal control formulation in Eq. (8) is discretised in the spectral domain, by projecting x and f_{u} onto a vector space of dimension N_{sp}, using a linear combination of orthogonal basis functions denoted as $\Phi = \phi_{i\,i=1}^{N_{sp}}$. For instance, the Fourier basis functions can be utilised. Consequently, the states and control force are approximated in the following manner:

$$\begin{aligned} x_i(t) &\approx x_i^{N_{sp}}(t) = \Phi^\intercal(t)\hat{\mathrm{x}}_i \\ f_{\mathrm{u}}(t) &\approx f_{\mathrm{u}}^{N_{sp}}(t) = \Phi^\intercal(t)\hat{\mathrm{f}}_{\mathrm{u}}, \end{aligned} \tag{9}$$

where coefficient vectors are defined as $\hat{x}_i = [x_{i1}\cdots x_{iN_{sp}}]^\intercal$, and $\hat{\mathrm{f}}_{\mathrm{u}} = [\mathrm{f}_{\mathrm{u}1}, \cdots \mathrm{f}_{\mathrm{u}N_{sp}}]^\intercal$, both $\in \mathbb{R}^{N_{sp}}$.

Within this (pseudo-)spectral framework, the equation of motion can be approximated as [17]:

$$\hat{\mathrm{v}} = \mathrm{G_o}(\hat{\mathrm{f}}_{\mathrm{ex}} - \hat{\mathrm{f}}_{\mathrm{u}}), \tag{10}$$

where $\hat{\mathrm{v}} = [v_1 \; v_2 \; \cdots \; v_{N_{sp}}]^\intercal$ denotes the coefficient vector for approximating the system velocity $v(t)$ and $\mathrm{G_o}$ represents the force-to-velocity system *model*. Additionally, in Eq. (10), $\hat{\mathrm{f}}_{\mathrm{ex}} = [\mathrm{f}_{\mathrm{ex}1}, \cdots \mathrm{f}_{\mathrm{ex}N_{sp}}]^\intercal \in \mathbb{R}^{N_{sp}}$, where the set $\{\mathrm{f}_{\mathrm{ex}i}\}_{i=1}^{N_{sp}}$ contains the coefficients of the excitation force approximation.

The primary objective of the optimal control problem is to determine the PTO control force $f_{\mathrm{u}}(t)$ that maximises the objective function presented in Eq. (7), while satisfying the equation of motion. Due to the mathematical properties of the basis functions Φ_j [20], the objective function in Eq. (7) can be approximated as follows:

$$E \approx J_N = \int_0^T \hat{\mathrm{f}}_{\mathrm{u}}^\intercal \Phi^\intercal(t)\Phi(t)\hat{\mathrm{v}} = -\frac{T}{2}\hat{\mathrm{f}}_{\mathrm{u}}^\intercal \hat{\mathrm{v}}, \tag{11}$$

which converts the integral relationship in Eq. (7) into an algebraic mapping. Then, using Eqs. (10) and (11), the objective function can be rewritten as:

$$J_N = -\frac{T}{2}\hat{\mathrm{f}}_{\mathrm{u}}^\intercal \mathrm{G_o}(\hat{\mathrm{f}}_{\mathrm{ex}} - \hat{\mathrm{f}}_{\mathrm{u}}). \tag{12}$$

1) Optimal solution:: Using (pseudo-)spectral methods, the control problem for WEC systems can now be described as follows:

$$\begin{aligned} \hat{\mathrm{f}}_{\mathrm{u}}^\star \leftarrow \max_{\hat{\mathrm{f}}_{\mathrm{u}} \in \mathbb{R}^N} \quad & J_N \\ \text{subject to:} \quad & \mathcal{C}, \end{aligned} \tag{13}$$

which is a standard quadratic optimisation problem over $\hat{\mathrm{f}}_{\mathrm{u}}$, and $\mathcal{C}$ represents a set of constraints arising from the physical limitations of the WEC system. In this study, specifically for the application case in Section VI, the maximum device displacement (X_{max}) can be considered for the definition of $\mathcal{C}$, as well as the maximum PTO force (F_{max}) or the maximum velocity (V_{max}). In general, the optimisation problem in Eq. (13), can be approached by forcing the constraints only at specific points in time ($\mathbf{T}_c = [t_1, t_2, \ldots t_{N_c}]$), which are labelled as collocation points. Then, considering X_{max} and F_{max}, being the most commonly considered constraints, the set $\mathcal{C}$, in Eq. (8), can be rewritten as a set of linear inequality constraints, as follows

$$\mathcal{C} := \begin{bmatrix} A_{\mathrm{u}} \\ A_X \end{bmatrix} \hat{\mathrm{f}}_{\mathrm{u}}^\intercal \leq \begin{bmatrix} b_{\mathrm{u}} \\ b_{\mathrm{X}} \end{bmatrix}, \tag{14}$$

where

$$\begin{aligned} A_{\mathrm{u}} &= \begin{bmatrix} \Phi(\mathbf{T}_c) \\ -\Phi(\mathbf{T}_c) \end{bmatrix}, \quad A_X = \begin{bmatrix} \Phi(\mathbf{T}_c)G_o \\ -\Phi(\mathbf{T}_c)G_o \end{bmatrix}, \\ b_{\mathrm{u}} &= \begin{bmatrix} F_{\mathrm{max}}\hat{\mathbf{1}} \\ F_{\mathrm{max}}\hat{\mathbf{1}} \end{bmatrix}, \quad b_X = \begin{bmatrix} X_{\mathrm{max}}\hat{\mathbf{1}} - \Phi(\mathbf{T}_c)\hat{\mathrm{f}}_{\mathrm{ex}} \\ X_{\mathrm{max}}\hat{\mathbf{1}} + \Phi(\mathbf{T}_c)\hat{\mathrm{f}}_{\mathrm{ex}} \end{bmatrix}, \end{aligned} \tag{15}$$

with $\hat{\mathbf{1}} \in \mathbb{R}^{2N_c \times 1}$ a column vector of ones. The problem stated in Eq. (13) can be solved with standard numerical toolboxes. Taking advantage of defined colocation points, general and standard multipurpose optimisation solvers (specifically QP-problem solvers) can be used to address the problem stated in Eq. (13), with the constraint definition in Eqs. (14) and (15).

IV. Hydrodynamic Coefficients Interpolation

This study proposes a parametric interpolation method for the design of the energy captor in WEC systems, specifically focusing on its geometrical and structural aspects. The approach utilises a pre-existing database of hydrodynamic coefficients that encompasses all possible variations in geometry. The database is generated using dedicated BEM tools, such as WAMIT [21], AQWA [22], or the open-source numerical solver NEMOH [15]. From a broad viewpoint, the computation of hydrodynamic coefficients is a time-consuming and computationally intensive task. This challenge becomes even more pronounced when computing hydrodynamic coefficients inside a CCD loop, particularly when combined with optimisation-based controllers, such as the spectral-based framework presented in Section III. While optimisation-based controllers offer the appealing advantage of providing optimal control solutions (in theory), their primary weakness lies in the significant computational burden they demand. This characteristic magnifies the challenge at hand and highlights the trade-off between optimal control and computational complexity. However, the attainment of optimal control solutions enables a comprehensive assessment of performance, particularly in terms of energy absorption, even in constrained and realistic scenarios. In contrast, impedance-matching-based control solutions, i.e. non-optimisation-based, by definition, are unable to address constraints, limiting their effectiveness in such scenarios. Hence, reducing the computational requirements involved in tasks such as computing hydrodynamic coefficients renders CCD with optimisation-based controllers more viable and appealing.

A. Database Generation and Interpolation

Based on Eqs. (5) and (6), the hydrodynamic coefficients $A_r(\omega)$, $B_r(\omega)$, M, and s_h play a crucial role in computing the force-to-velocity mapping, required for solving the control problem described in Eq. (8). Additionally, the mapping between wave height-elevation and excitation force, $\mathcal{H}_{\mathrm{ex}}(\omega)$, is also required for the assessment of an energy-maximising controller.

The methodology presented here acknowledges that a certain degree of error between a hydrodynamic coefficient value, obtained through interpolation, and the actual value, from the BEM computational tool, is acceptable. However, it should be emphasised that capturing infinitesimal variation of the hydrodynamic coefficient across the entire range of considered variations requires an infinite number of iterations with the BEM tool, which can be in a large number of applications prohibitive. Fig. 1 illustrates the underlying general concept of the proposed methodology. A schematic representation of a generic hydrodynamic parameter P, as a function of a specific geometrical parameter ρ, is shown in Fig. 1. The solid line in Fig. 1 represents the variations of P within a given interval of variations

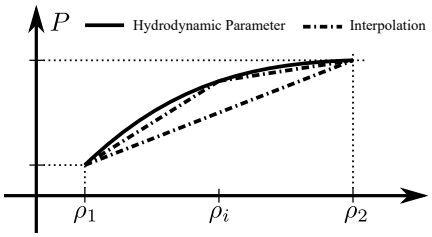

Fig. 1. Schematic illustration of the proposed binary search method for a unidimensional case.

defined by ρ_1 and ρ_2. On the other hand, the dashed-dotted line represents two alternative linear interpolations: one connecting the interval extremes and another employing a two-segment linear interpolation with an intermediate point ρ_i. It is worth noting that BEM-based tools represent hydrodynamic parameters in the spectral domain using a discrete set of frequencies. By way of example, considering the case described in Fig. 1, the parameter ρ can describe any geometrical measure, such as radius, length, draft, etc. Therefore, the frequency domain of hydrodynamic parameters can be expressed as:

$$\Omega = \begin{bmatrix} \omega_1, & \dots, & \omega_{N_\omega} \end{bmatrix}. \tag{16}$$

Considering a general parameter $\rho \in \mathbb{R}^N$ that describes a set of geometrical measures, the key hydrodynamic parameters in the force-to-velocity mapping, as defined in Eqs. (5) and (6) for transfer function and impedance representations, respectively, include:

$$[A_{\mathrm{r}}(\omega,\rho), \quad B_{\mathrm{r}}(\omega,\rho), \quad M(\rho), \quad s_{\mathrm{h}}(\rho), \quad \mathcal{H}_{\mathrm{ex}}(\omega,\rho)], \tag{17}$$

which represent the added mass, radiation damping, mass, stiffness, and wave height elevation-to-excitation force mapping, respectively. Thus, Eq. (17), describe the key hydrodynamic parameters as functions of the frequency $\omega \in \Omega$ and the geometrical variation parameter ρ. For a specific frequency $\omega^\star \in \Omega$, the hydrodynamic parameters can be expressed as functions solely dependent on the parameter ρ, as follows:

$$[A_{\mathrm{r}}(\omega^\star,\rho), \quad B_{\mathrm{r}}(\omega^\star,\rho), \quad M(\rho), \quad s_{\mathrm{h}}(\rho), \quad \mathcal{H}_{\mathrm{ex}}(\omega^\star,\rho)]. \tag{18}$$

Considering a single DoF WEC for the sake of simplificity, as defined in Section II, but without loss of generality, each parametrised hydrodynamic coefficient by the parameter ρ, defines $N-$dimensional mapping

$$\mathcal{C}_h : \mathbb{R}^N \mapsto \mathbb{R}, \tag{19}$$

where h can be replaced by A_{r}, B_{r}, M, s_{h}, and $\mathcal{H}_{\mathrm{ex}}$, depending on the case. Thus, each hydrodynamic coefficient represents a multidimensional real function describing a hyper-surface. To define the dataset used as database, in this study, the parameter vector ρ is discretised to define a grid in a hypercube, as follows:

$$\mathcal{P} = \begin{Bmatrix} \rho_1, & \dots & \rho_{N_\rho} \end{Bmatrix}. \tag{20}$$

Thus, each hydrodynamic parameter is computed using a BEM-based tool for each ρ_i, with $i = 1, 2, \dots, \rho_{N_\rho}$, to compute the predefined database.

With the precomputed database, an intermediate value between two consecutive points on the grid $\mathcal{P}$, namely ρ_i and ρ_{i+1}, can be determined using various interpolation methods, such as linear or spline interpolation. Alternatively, a parametric hyper-surface can be fitted to minimise the least-mean-square (LMS) error, representing a common curve-fitting problem. Thus, a WEC system, described, for example, using its transfer function representation can be approximated as:

$$G(\jmath\omega,\rho^\star) \approx \hat{G}(\jmath\omega,\rho^\star), \tag{21}$$

where, considering a generic $\rho^\star \in \mathcal{P}$, $G(\jmath\omega,\rho^\star)$ denotes the actual WEC system representation, computed using BEM-based tools, while $\hat{G}(\jmath\omega,\rho^\star)$ is obtained using the interpolating or fitted functions.

An immediate consequence of Eq. (21) is the possibility of achieving a small approximation error, denoted as ϵ_G, by appropriately defining a sufficiently large set $\mathcal{P}$, i.e.

$$\|G(\jmath\omega,\rho^\star) - \hat{G}(\jmath\omega,\rho^\star)\| = \epsilon_G. \tag{22}$$

This error represents the discrepancy between the true system response $G(\jmath\omega,\rho^\star)$ and its approximation $\hat{G}(\jmath\omega,\rho^\star)$. By selecting a comprehensive set of parameter values in $\mathcal{P}$, the accuracy of the approximation can be controlled and improved, ensuring that the error remains within acceptable limits. In addition, and by way of example, it is worth highlighting that in cases where the variation of hydrodynamic parameters exhibits a certain level of linearity, a single linear interpolating hyper-plane can be effectively employed, guaranteeing a negligible level of error, i.e small ϵ_G. This characteristic of the approach enhances its appeal, as it allows for simplified and efficient approximation techniques while maintaining a satisfactory level of accuracy. In the illustrative example depicted in Fig. 1, it can be observed that using three elements in the grid yields a satisfactory level of approximation. However, it is important to note that reducing the number of parameter points to only two can result in a notable approximation error at ρ_i. This highlights the importance of carefully selecting the number of parameters and grid elements to ensure an accurate interpolation in the desired range.

V. Structural Optimisation for Control Co-Design Approach

A. CCD Problem Statement

In the context of CCD schemes, with a specific focus on geometrical optimisation, the optimisation problem can be formulated as follows:

$$\begin{aligned} \rho^{\mathrm{opt}} \leftarrow \quad & \underset{\rho\in\mathbb{R}^N}{\text{Optimise}} && \Psi \\ & \text{subject to:} \quad \underset{\hat{\mathrm{f}}_{\mathrm{u}}\in\mathbb{R}^N}{\max} && J_N(\rho) \\ & && \mathcal{C} \end{aligned} \tag{23}$$

where the optimisation (minimisation or maximisation) is performed depending on the particular objective function Ψ considered, solely over the variable ρ. Thus, Ψ can be defined depending on the specifications of the application. In particular, Ψ can be designed to provide

an assessment of energy absorption per unit of mass, which can be expressed as follows:

$$\Psi = \frac{E(\rho)}{w(M(\rho))} \tag{24}$$

where function $w(\cdot)$, with $w : \mathbb{R}^N \mapsto \mathbb{R}$, a weighting function, that allows for the consideration of various factors, such as the price of materials, manufacturing costs, or other relevant considerations. By incorporating the weighting function, the optimisation objective can be balanced to account for different aspects and priorities in the design process. Alternatively, Ψ can be defined similarly to the approach presented in [5], which assesses the interplay between the total cost (CapEx+OpEx) and energy absorption. Within this context, the expression for Ψ is as follows:

$$\Psi = \frac{\text{CapEx}(\rho) + \text{OpEx}(\rho)}{E(\rho)}. \tag{25}$$

In this formulation, by considering the total cost in the numerator and the energy absorption in the denominator, the objective function captures the trade-off between the economic factors and the energy performance of the WEC. However, in order to use this objective function, both the CapEx and OpEx need to be parameterised as functions of ρ, as performed, considering PTO constraints, in [5]. Thus, this parameterisation allows for the assessment of different design configurations in terms of their cost-effectiveness and energy absorption potential.

B. Problem Solution

The problem stated in Eq. (23) can be approached in a number of different ways. As discussed in [23], different methods for solving CCD problems can be found in the literature, where three primary methods, defines as lines (L), can be identified: (L1) control-inspired paradigms, (L2) co-optimisation techniques, and (L3) co-simulation methods. The control-inspired paradigms (L1) approach utilises engineering understanding of dynamics and control principles. It employs low-fidelity models (control-oriented models) and control engineering tools to propose new mechanisms, networks, and control solutions based on the system control properties. The co-optimisation techniques (L2) employ formal mathematical methodologies with nonlinear models and optimisation theory. Initially focused on fixed-structure controllers and plants, it later expanded to allow changes in these structures during the optimisation process. It involves multi-objective constrained optimisation and considers the cost function of the plant architecture, dynamics, and controller design. Finally, the co-simulation-based methods (L3), which use high/mixed-fidelity dynamic models in an iterative simulation process, can also incorporate optimisation algorithms, data-based models, and machine learning techniques.

In particular, co-simulation methods offer advantages in CCD problems compared to lines L1 and L2 [23]. In particular, the complexity of CCD problems can rapidly escalate, leading to an exponential increase in the number of design possibilities. This exponential growth can make analytical treatments impractical and computationally prohibitive for finding optimal solutions. In contrast, the key advantages of co-simulation include the ability to integrate multiscale and multi-physics models, perform iterative simulations for design refinement, incorporate optimisation algorithms and data-driven/machine learning techniques, and provide a flexible and modular design approach. These features enable a comprehensive analysis of system dynamics, efficient exploration of design options, and reduced design cycle time, making co-simulation an effective methodology for finding optimal solutions in CCD problems. The interested reader is referred to [23] for a detailed discussion about CCD solution methodologies.

In order to address the problem described in Subsection V-A, in Eq. (23), this study proposes a methodological solution based on a co-simulation approach combined with a binary search algorithm. This approach aims to leverage the advantages offered by the interpolation methodology discussed earlier, allowing for efficient exploration of the solution space. A similar methodology, exclusively based on an exhaustive search procedure, is considered for the study presented in [5].

1) Binary Search Method: The binary search algorithm for N-dimensional problems using binary space partitioning (BSP) is a recursive technique that efficiently explores the search space. The algorithm can be summarised as follows:

1: **Define the search space.** The dimension of the search space, N, is given by dimension of by $\rho \in \mathbb{R}^N$, while the search criterion, or objective function, is defined as $\Psi : R^N \to \mathbb{R}$.
2: **Choose a splitting criterion.** Determine a splitting criterion based on the problem features. One approach could involve dividing each dimension in half at each iteration, effectively exploring the solution space by systematically reducing the search domain.
3: **Split the search space.** Divide the N-dimensional space $\mathcal{P}$ into two sub-regions $\mathcal{P}_1$ and $\mathcal{P}_2$ using the chosen splitting criterion.
4: **Evaluate the sub-regions.** Evaluate the search criterion or objective function Ψ for each sub-region $\mathcal{P}_1$ and $\mathcal{P}_2$.
5: **Choose the sub-region to explore.** Select the sub-region candidate, which means being more favourable ('promising'), based on the evaluation in step 4 ($\mathcal{P}_1$ or $\mathcal{P}_2$). This sub-region becomes the new search space. By focusing the search on the more favourable areas of the solution space, the algorithm aims to converge towards an optimal solution more effectively.
6: **Repeat steps 3-5.** Repeat steps 3 to 5 for the selected sub-region until a termination condition is met.
7: **Return the solution.** Once the termination condition is met, return the solution found in the final sub-region.

The considered algorithm is an extension of the binary search concept to N-dimensional problems, al-

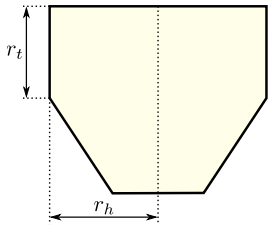

Fig. 2. Schematic of the considered buoy with the most relevant dimensions, required for the presented CCD analysis.

lowing for efficient exploration of the search space [24]. It has been successfully applied in various engineering domains, such as optimisation and computational geometry [25], [26]. This approach facilitates the direct integration and utilisation of the interpolating or fitting hyper-surfaces discussed in Section IV. Finally, BSP exhibits a time complexity $O(\log N)$[1]. This efficiency arises from the ability to divide the search space in half at each iteration, effectively reducing the search domain by half with each step. As a result, binary search can efficiently locate the desired element or region within a sorted or partitioned space, making it an effective algorithm for searching and optimization problems.

VI. Case Study

This section presents an illustrative example, which covers the methodology discussed throughout Sections V and IV. The illustrative example considers a point-absorber type WEC system, where the geometry of the system is defined by varying two structural measures. The WEC system is schematically presented in Fig. 2, indicating the two variable quantities, r_t and r_h, where $r_t \in [0, 10]$ and $r_h \in [0, 8]$. As shown in Fig. 2, the considered system spans a range from a pure cone, when $r_t = r_h = 0$, to a pure cylinder, when both r_t or r_h are fully deployed. With this structural definition. The pre-computed database is generated in this study considering:

$$\begin{aligned} r_t &\in \{0, \quad 2.5, \quad 5, \quad 7.5, \quad 10\} \\ r_h &\in \{0, \quad 2, \quad 4, \quad 6, \quad 8\}. \end{aligned} \tag{26}$$

Consequently, a grid compromised with 25 systems is precomputed. Based on the grid definition in Eq. (26), each hydrodynamic coefficient, indicated in Eq. (17) for computing the force-to-velocity mapping in Eq. (5), is computed using NEMOH [15]. By way of example, the structural grid and pressure field used for NEMOH, considering one particular semi-cylinder-conic geometry case, is shown in Fig. 3. Particularly, Fig. 4 illustrates the resulting mass for each system in the grid, represented using solid dots. Inn particular, Fig. 4 clearly indicates that the configuration with the larger mass corresponds to the cylindrical case ($r_t = 10$ m and $r_h = 8$ m), while the configuration with the smaller mass is associated with the conical structure ($r_t = 0$ m and $r_h = 0$ m). Similarly, in Fig. 5 the resulting force-to-velocity mapping, as defined in Eq. (6), is shown in

[1]See, for example, [24], Chapter 2, particularly Section 2.3: "Divide-and-Conquer".

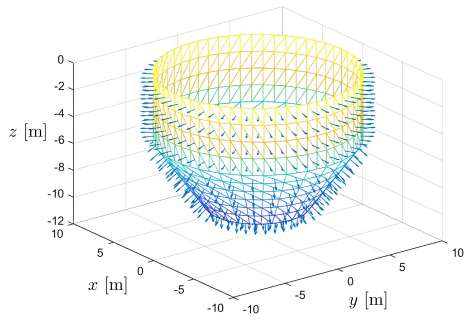

Fig. 3. Structural mesh and pressure considered in NEMOH for subsequent interpolation: Semi-cylinder-conic geometry, specifically intermediate cylinder-cone configuration.

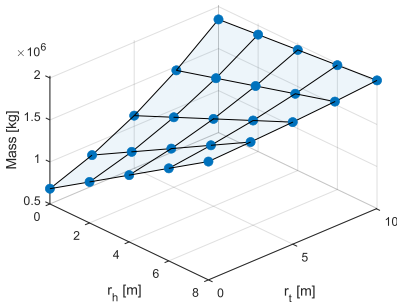

Fig. 4. Resulting mass for each system in the grid, represented using solid dots.

Figures (5)(a), (b), and (c), using the top and the bottom rows for the magnitude and phase, respectively. For each system in the precomputed grid, Fig. 5(a) shows the specific case where $r_h = 0$ m, with a colour scale ranging from lighter to deeper blue, which represents the variation from $r_t = 0$ m to $r_t = 10$ m. Similarly, in Fig. 5(b), the specific case where $r_t = 0$ m is depicted, with a colour scale ranging from lighter to deeper orange, representing the variation from $r_h = 0$ m to $r_h = 8$ m. Finally, in Fig. 5(c) all the cases indicated in Eq. (26) are shown using solid-grey lines. It must be noted that, as a consequence of using NEMOH, some irregularities are obtained for specific frequencies. This phenomenon has been widely discussed in the literature. Consequently, diverse methods have been presented to mitigate this effect, and 'smooth' the obtained description for each hydrodynamic parameter [27]. In this study, the irregular responses have been smoothed, to obtain regular and realistic descriptions of the hydrodynamic coefficients.

For the CCD optimisation problem, waves based on a JONSWAP spectrum [28], with a significant wave height $H_s = 3$ m, peak period $T_p = 12$ s, and steepness factor $\gamma = 3.3$, are considered. In addition, considered waves are synthesised using filtered white noise [29]. To produce statistically consistent results, 10 realisations of the considered sea-state are used. Each simulation is performed over 200 s, which represents 20 times the peak period of the considered sea-state. The optimisation problem, for computation of the optimal control force, expressed in Eq. (13), is solved via an interior-point method, using the Optimisation Toolbox in Matlab R2022a. Ultimately, in the control problem, stated in Eq. (13), position constraints $X_{\max} = H_s = 3$

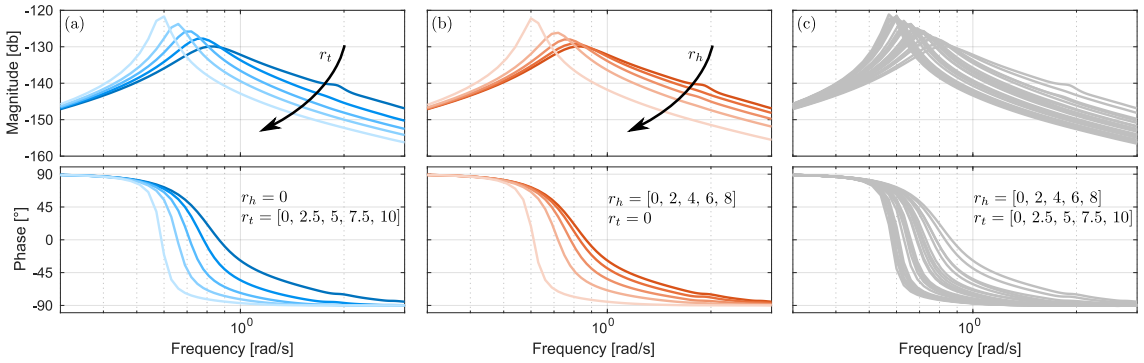

Fig. 5. Resulting force-to-velocity mapping, as defined in Eq. (6). The specific cases $r_t = 0$ m and $r_h = 0$ m, are shown in (a) and (b), respectively. In (c) all the cases in Eq. (26) are illustrated.

m, are considered to consider a realistic operation scenario, preserving the physical integrity of the WEC system.

The spectral-based control strategy is applied to each system in the grid, and the average absorbed energy for each system is shown in Fig. 6. It is worth noting

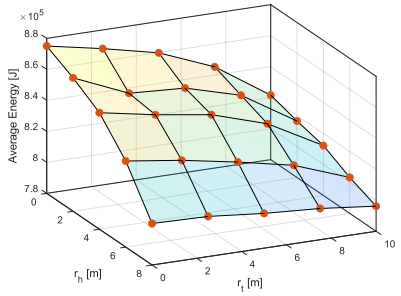

Fig. 6. Average absorbed energy for each system in the grid.

that, from the results shown in Fig. 6, the conical case, characterised by the smallest mass, achieves the highest absorbed energy value.

A. CCD Scheme Application.

The CCD methodology for geometrical optimisation is applied in two distinct scenarios, employing the objective function defined as in Eq. (24). The first scenario assumes a flat weighting function $w(\cdot)$, meaning no mass scaling is applied. In the second scenario, a non-flat weighting function $w(\cdot)$ is used, exploring the performance of the algorithm in a different context. It is important to note that the presented weighting function does not possess a specific physical interpretation. Rather, it serves the purpose of showcasing the performance of the CCD methodology in an alternative scenario. Under this framework, the two scenarios are defined by:

$$\begin{aligned} w_{S1}(r_t, r_h) &= 1, \\ w_{S2}(r_t, r_h) &= \frac{1}{10}(r_t - 2)^2 + \frac{1}{8}(r_h - 2)^2) + 1, \end{aligned} \tag{27}$$

As mentioned before, in Scenario 1 (denoted as $S1$), a flat weighting function of 1 is employed. On the other hand, in Scenario 2 (denoted as $S2$), the weighting function $w_{S2}(r_t, r_h)$ is utilised, incorporating a quadratic term, in order to achieve an unbalanced mass distribution. It is important to recall that these weighting functions are specifically designed for the purpose of defining the scenarios and do not necessarily have a direct physical interpretation.

The methodology is applied in S1 and S2. In Fig 7 each sub-region of the complete variation set $\mathcal{P}$ is shown, in accordance with the algorithm described in Section V-B1, where each successive sub-region, $\mathcal{P}_i$, is indicated using deeper to lighter blue coloured boxes.

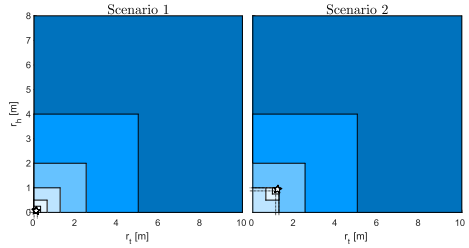

Fig. 7. Each sub-region of the complete variation set $\mathcal{P}$ is shown. Each successive sub-region, $\mathcal{P}_i$, is indicated using deeper to lighter blue coloured boxes.

In Fig. 7 the results for S1 and S2 are depicted on the left- and right-hand side panels, respectively. The as indicated in the algorithm in Section V-B1, a termination condition c is defined for the results in Fig. 7 as follows:

$$c = \sqrt{l_t l_h} < 0.1, \tag{28}$$

where l_h and l_t represent the length of each side, corresponding to r_h and r_t axes, respectively, of each rectangle in Fig. 7. Thus, the solution is found for S1 and S2 at:

$$\begin{aligned} 0 \leq r_h \leq 0.12500 \\ 0 \leq r_t \leq 0.15625, \end{aligned} \tag{29}$$

and

$$\begin{aligned} 0.87500 \leq r_h \leq 1.00000 \\ 1.09380 \leq r_t \leq 1.25000, \end{aligned} \tag{30}$$

for S1 and S2, respectively. In Fig. 7 the optimal value found is indicated with a star symbol. On the one hand, it can be easily concluded that the maximum value for S1 is located on the corner that defines the conical case, i.e.

$$1.283 = \rho_{S1}^{opt} \leftarrow (0,\, 0)\,. \tag{31}$$

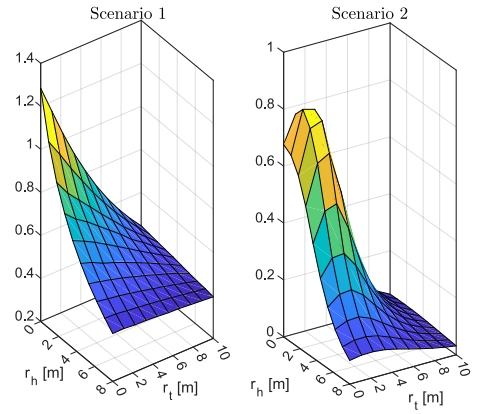

Fig. 8. CCD results considering a grid with 121 elements. The problem for this grid is computed using an exhaustive search methodology.

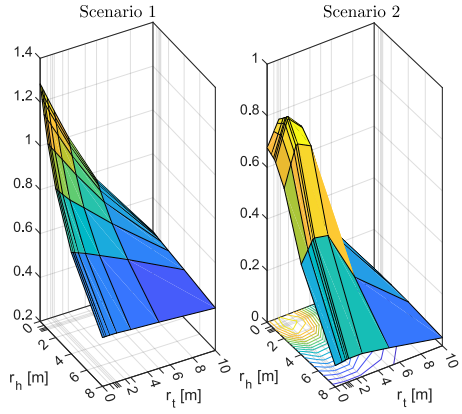

Fig. 9. The plot highlights the effectiveness of utilizing a binary search method with interpolation based on a precomputed dataset, as it yields comparable outcomes to those obtained through an exhaustive search-based approach. Specifically, the refined grid resulting from the application of the binary search method can be observed for scenarios 1 and 2

On the other hand, the optimal solution for S2 is found within the considered range of variation. With the estimated limits for the optimal value defined in Eq. (30), the optimal value can be approximated by taking the average of the values on the limits (corners), as well as the average of the objective function on the corners, of the last computed rectangle:

$$0.783 = \rho_{S2}^{opt} \leftarrow (0.9397,\, 1.1719)\,. \tag{32}$$

For the sake of validation, considering a finer mesh, specifically designed for validating the presented approach, is designed considering 11 points, instead of 5 as considered for the original grid, for r_t and r_h, which gives to 121 elements in the grid. The results are obtained by evaluating the absorbed energy for each element in the grid and computing the value of the objective function, as defined in Eq.(24), for both S1 and S2. The results of this exhaustive search procedure are depicted in Fig. 8, with the results for S1 and S2 shown in the left- and right-hand side panels, respectively.

It is noteworthy that the results obtained using the finer mesh are approximately equivalent to those obtained using the binary search methodology. For S1, the optimal solution is found at $(r_h, , r_t) = (0, , 0)$, with an optimal value of 1.283. Similarly, for S2, the optimal solution is located at $(r_h, , r_t) = (0.888, , 1.111)$, yielding an optimal value of 0.806. Thus, the results obtained with the exhaustive search methodology are approximately equivalent to those obtained with the binary search method. However, it should be noted that the number of points evaluated using the binary search method is significantly lower, with only 28 evaluations (7 rectangles, each with 4 vertices), compared to the full grid evaluation method which requires 121 system evaluations. Similar to the results shown in Fig. 8, the CCD results illustrated in Fig. 7 are visualised using a surface plot in Fig. 9. The non-regular mesh, resulting from the grid definition based on each subregion $\mathcal{P}_i$, is clearly visible, showcasing its effect on the optimization process. It must be mentioned that, in general, the binary search method, like other optimisation methods, is not immune to the possibility of encountering local maxima or minima. This means that in certain cases, the method may converge to

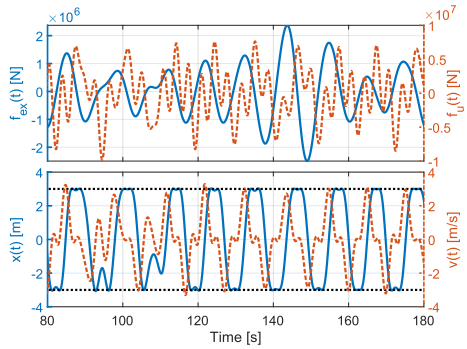

Fig. 10. Control results for one particular case (cylindrical case). The capability of the controller, to strictly adhere to the specified physical constraints, is shown.

suboptimal solutions instead of the global optimum. However, it is important to note that this weakness does not only belong to the binary search method. Even standard optimization methods based on, for example, gradient search, or similar techniques, can also suffer from the same limitation. The presence of local extrema is a common challenge in optimisation problems, and various strategies are employed, such as incorporating randomization or exploring multiple starting points, to mitigate the risk of obtaining local (sub) optima. Therefore, while the binary search method may exhibit this weakness, it is a characteristic shared by many optimisation approaches, in general. In particular, Fig. 7 highlights the effectiveness of utilising a binary search method with interpolation based on a precomputed dataset, as it yields comparable outcomes to those obtained through an exhaustive search-based approach. Specifically, the refined grid resulting from the application of the binary search method can be observed for scenario 1 and 2, in Fig. 7.

Finally, by way of example, the control results for one particular case (cylindrical case), are shown in Fig. 10, where the motion of the device (bottom), i.e. $x(t)$ and $v(t)$, along with both f_{u} and f_{ex} (top), for a given sea-state realisation, confirming the capability of the controller in strictly adhering to the specified physical constraints.

VII. Conclusion

This study presents a novel methodology for addressing CCD problems in WEC systems, with a specific focus on geometrical optimization. The effectiveness and efficiency of the methodology are demonstrated through two stages involving database precomputation and interpolation-based strategies. Notably, the presented approach avoids the use of BEM tools in online computation, resulting in significantly reduced computational complexity. The results of the illustrative example in Section VI show that the proposed method substantially reduces the numerical burden compared to exhaustive search-based approaches (in at least 25%). Moreover, the versatility of the presented methodology allows for easy adaptation to alternative problem formulations, regardless of the number of parametrization variables or the control strategy employed. By increasing the number of elements in the precomputed dataset grid, the approximation error can be minimized, further enhancing the accuracy of the methodology. In realistic cases where BEM computation times are longer, the presented approach remains advantageous. The number of required runs is limited, and the level of nonlinearity determines the need for proper interpolation. For real design scenarios covering a range of sea-states (combinations of T_p and H_s), more cases will be involved. However, the proposed method remains attractive as the amount of computation is consistently reduced, making it an efficient tool for comprehensive and realistic analyses. In summary, the contribution of this study lies in the development of a methodology that effectively addresses CCD in WEC systems, with a focus on geometrical optimization. By substantially reducing the numerical burden, this approach enables the easier implementation of control co-design methods, making it a valuable tool for real-world applications.

References

[1] P. Stansby, E. C. Moreno, and T. Stallard, "Large capacity multi-float configurations for the wave energy converter M4 using a time-domain linear diffraction model," *Applied Ocean Research*, vol. 68, pp. 53–64, 2017.

[2] J. V. Ringwood, "Wave energy control: status and perspectives 2020," *IFAC-PapersOnLine*, vol. 53, no. 2, pp. 12 271–12 282, 2020, 21st IFAC World Congress. [Online]. Available: https://www.sciencedirect.com/science/article/pii/S2405896320315536

[3] A. Mérigaud and J. V. Ringwood, "Improving the computational performance of nonlinear pseudospectral control of wave energy converters," *IEEE Transactions on Sustainable Energy*, vol. 9, no. 3, pp. 1419–1426, 2018.

[4] R. G. Coe, G. Bacelli, S. Olson, V. S. Neary, and M. B. R. Topper, "Initial conceptual demonstration of control co-design for wec optimization," *Journal of Ocean Engineering and Marine Energy*, vol. 6, no. 4, pp. 441–449, 2020. [Online]. Available: https://doi.org/10.1007/s40722-020-00181-9

[5] Y. Peña-Sanchez, D. García-Violini, and J. V. Ringwood, "Control co-design of power take-off parameters for wave energy systems," *IFAC-PapersOnLine*, vol. 55, no. 27, pp. 311–316, 2022, 9th IFAC Symposium on Mechatronic Systems MECHATRONICS 2022. [Online]. Available: https://www.sciencedirect.com/science/article/pii/S2405896322025848

[6] P. B. Garcia-Rosa, G. Bacelli, and J. V. Ringwood, "Control-informed optimal array layout for wave farms," *IEEE Transactions on Sustainable Energy*, vol. 6, no. 2, pp. 575–582, 2015.

[7] M. Neshat, B. Alexander, N. Y. Sergiienko, and M. Wagner, "A hybrid evolutionary algorithm framework for optimising power take off and placements of wave energy converters," in *Proceedings of the Genetic and Evolutionary Computation Conference*, 2019, pp. 1293–1301.

[8] P. B. Garcia-Rosa and J. V. Ringwood, "On the sensitivity of optimal wave energy device geometry to the energy maximizing control system," *IEEE Transactions on Sustainable Energy*, vol. 7, no. 1, pp. 419–426, 2015.

[9] R. E. D. Bishop, W. G. Price, and P. K. Y. Tam, "Hydrodynamic confficients of some heaving cylinders of arbitrary shape," *International Journal for Numerical Methods in Engineering*, vol. 13, no. 1, pp. 17–33, 1978. [Online]. Available: https://onlinelibrary.wiley.com/doi/abs/10.1002/nme.1620130103

[10] E. Jefferys, "Interpolation and extrapolation of hydrodynamic coefficients," *Applied Ocean Research*, vol. 5, no. 3, pp. 145–149, 1983. [Online]. Available: https://www.sciencedirect.com/science/article/pii/014111878390069X

[11] W. E. Cummins, "The impulse response function and ship motions," *Schiffstechnik*, vol. 47, pp. 101–109, 1962.

[12] T. F. Ogilvie, "Recent progress toward the understanding and prediction of ship motions," in *5th Symposium on Naval Hydrodynamics*, vol. 1. Bergen, Norway, 1964, pp. 2–5.

[13] J. Falnes, *Ocean waves and oscillating systems: linear interactions including wave-energy extraction*. Cambridge Univ. Press, 2002.

[14] D. García-Violini, Y. Peña-Sanchez, N. Faedo, and J. V. Ringwood, "An energy-maximising linear time invariant controller (LiTe-Con) for wave energy devices," *IEEE Transactions on Sustainable Energy*, vol. 11, no. 4, pp. 2713–2721, 2020.

[15] LHEEA, NEMOH-Presentation, "Laboratoire de Recherche en Hydrodynamique Énergetique et Environnement Atmospherique," https://goo.gl/yX8nFu, 2017, [Online accessed 1-Aug-2019].

[16] N. Faedo, Y. Peña-Sanchez, and J. V. Ringwood, "Finite-order hydrodynamic model determination for wave energy applications using moment-matching," *Ocean Engineering*, vol. 163, pp. 251–263, 2018.

[17] D. Garcia-Violini and J. V. Ringwood, "Energy maximising robust control for spectral and pseudospectral methods with application to wave energy systems," *International Journal of Control*, vol. 94, no. 4, pp. 1102–1113, 2021.

[18] N. Faedo, S. Olaya, and J. V. Ringwood, "Optimal control, MPC and MPC-like algorithms for wave energy systems: An overview," *IFAC Journal of Systems and Control*, vol. 1, pp. 37–56, 2017.

[19] G. Bacelli and J. V. Ringwood, "Numerical optimal control of wave energy converters," *IEEE Transactions on Sustainable Energy*, vol. 6, no. 2, pp. 294–302, 2014.

[20] D. García-Violini, M. Farajvand, C. Windt, V. Grazioso, and J. V. Ringwood, "Passivity considerations in robust spectral-based controllers for wave energy converters," in *2021 XIX Workshop on Information Processing and Control (RPIC)*. IEEE, 2021, pp. 1–6.

[21] WAMIT, "Wamit," https://www.wamit.com, 202023, online accessed 1-Jun-2023.

[22] AnsysAqwa, "AnsysAqwa," https://https://www.ansys.com/products/structures/ansys-aqwa, 2023, online accessed 1-Jun-2023.

[23] M. Garcia-Sanz, "Control co-design: an engineering game changer," *Advanced Control for Applications: Engineering and Industrial Systems*, vol. 1, no. 1, p. e18, 2019.

[24] T. H. Cormen, C. E. Leiserson, R. L. Rivest, and C. Stein, *Introduction to algorithms*. MIT press, 2022.

[25] S. P. Boyd and L. Vandenberghe, *Convex optimization*. Cambridge university press, 2004.

[26] M. De Berg, M. Van Kreveld, M. Overmars, O. Schwarzkopf, M. de Berg, M. van Kreveld, M. Overmars, and O. Schwarzkopf, *Computational Geometry: Introduction*. Springer, 1997.

[27] T. Kelly, I. Zabala, Y. Pena-Sanchez, M. Penalba, J. Ringwood, J. Henriques, and J. Blanco, "A post-processing technique for addressing 'irregular frequencies' and other issues in the results from bem solvers," in *Proceedings of the 14th European Wave and Tidal Energy Conference 5-9th Sept 2021, Plymouth, UK*, 2021.

[28] K. Hasselmann, "Measurements of wind wave growth and swell decay during the Joint North Sea Wave Project (JONSWAP)," *Deutches Hydrographisches Institut*, vol. 8, p. 95, 1973.

[29] M. Tucker, P. G. Challenor, and D. Carter, "Numerical simulation of a random sea: a common error and its effect upon wave group statistics," *Applied ocean research*, vol. 6, no. 2, pp. 118–122, 1984.